Article

Cell Reports

Long-Term Consolidation of Ensemble Neural Plasticity Patterns in Hippocampal Area CA1

Graphical Abstract

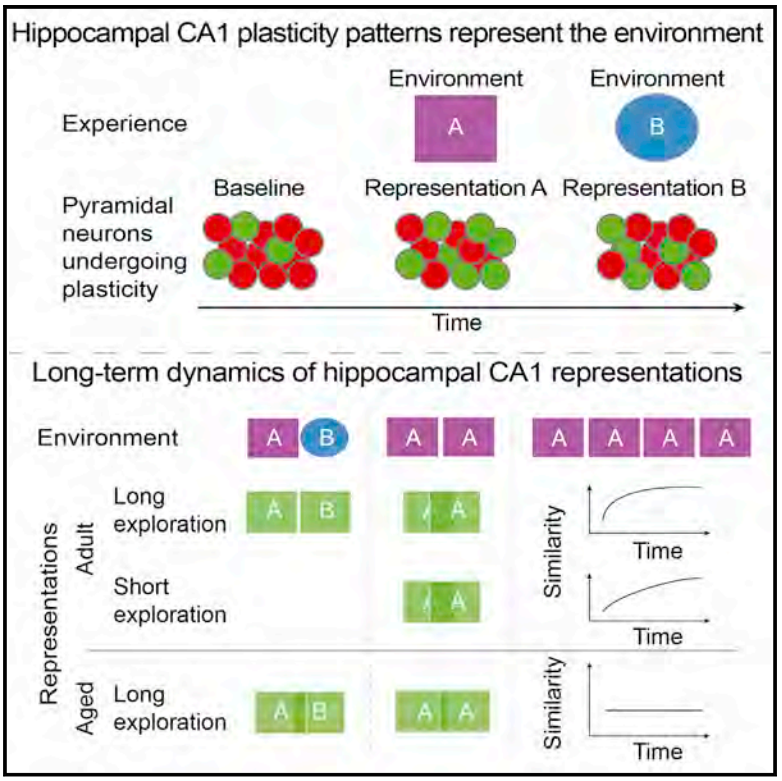

Authors

Alessio Attardo, Ju Lu, Takashi Kawashima, Hiroyuki Okuno, James E. Fitzgerald, Haruhiko Bito, Mark J. Schnitzer

Correspondence

alessio_attardo@psych.mpg.de (A.A.), mschnitz@stanford.edu (M.J.S.)

In Brief

Attardo et al. use a fluorescent reporter of neural plasticity to image ensemble plasticity patterns in hippocampal neurons of live mice. These patterns turn over but progressively stabilize across repeated explorations of an enriched environment. In aged mice, plasticity patterns do not stabilize and are less specific to individual environments.

Highlights

- Long-term imaging of hippocampal neural ensemble plasticity patterns in live mice
- Plasticity patterns in hippocampal area CA1 encode specific behavioral episodes
- Over repeat episodes, CA1 plasticity patterns turn over but progressively stabilize
- Aging degrades the stability and specificity of plasticity patterns

Attardo et al., 2018, Cell Reports *25*, 640–650
October 16, 2018
https://doi.org/10.1016/j.celrep.2018.09.064

CellPress

OPEN ACCESS
CellPress

Cell Reports
Article

Long-Term Consolidation of Ensemble Neural Plasticity Patterns in Hippocampal Area CA1

Alessio Attardo,[1,2,3,4,*] Ju Lu,[1,7] Takashi Kawashima,[5,8] Hiroyuki Okuno,[5,9] James E. Fitzgerald,[1,8] Haruhiko Bito,[5,6] and Mark J. Schnitzer[1,2,3,10,*]

[1]James H. Clark Center for Biomedical Engineering & Sciences, Stanford University, Stanford, CA 94305, USA
[2]Howard Hughes Medical Institute, Stanford University, Stanford, CA 94305, USA
[3]CNC Program, Stanford University, Stanford, CA 94305, USA
[4]Department of Stress Neurobiology and Neurogenetics, Max Planck Institute of Psychiatry, 80804 Munich, Germany
[5]Department of Neurochemistry, Graduate School of Medicine, The University of Tokyo, Bunkyo-ku, Tokyo 113-0033, Japan
[6]CREST-AMED, Chiyoda-ku, Tokyo 100-0004, Japan
[7]Present address: Department of Molecular, Cell and Developmental Biology, University of California, Santa Cruz, Santa Cruz, CA 95064, USA
[8]Present address: Howard Hughes Medical Institute (HHMI), Janelia Research Campus, Ashburn, VA 20147, USA
[9]Present address: Department of Biochemistry and Molecular Biology, Graduate School of Medical and Dental Sciences, Kagoshima University, Kagoshima 890-8544, Japan
[10]Lead Contact
*Correspondence: alessio_attardo@psych.mpg.de (A.A.), mschnitz@stanford.edu (M.J.S.)
https://doi.org/10.1016/j.celrep.2018.09.064

SUMMARY

Neural network remodeling underpins the ability to remember life experiences, but little is known about the long-term plasticity of neural populations. To study how the brain encodes episodic events, we used time-lapse two-photon microscopy and a fluorescent reporter of neural plasticity based on an enhanced form of the synaptic activity-responsive element (E-SARE) within the *Arc* promoter to track thousands of CA1 hippocampal pyramidal cells over weeks in mice that repeatedly encountered different environments. Each environment evokes characteristic patterns of ensemble neural plasticity, but with each encounter, the set of activated cells gradually evolves. After repeated exposures, the plasticity patterns evoked by an individual environment progressively stabilize. Compared with young adults, plasticity patterns in aged mice are less specific to individual environments and less stable across repeat experiences. Long-term consolidation of hippocampal plasticity patterns may support long-term memory formation, whereas weaker consolidation in aged subjects might reflect declining memory function.

INTRODUCTION

A rich literature has identified cellular and molecular bases for neural plasticity thought to support long-term memory (Bailey and Kandel, 1993; Caroni et al., 2012; Rogerson et al., 2014). Neural electrical activity induces transcription of immediate-early genes (IEGs), which initiate structural and functional cellular changes (Leslie and Nedivi, 2011; West and Greenberg, 2011). Studies of plasticity have generally focused on how individual cells change on timescales of minutes to hours, but it is equally vital to study plasticity at the network level and over the long term.

Here we examined long-term plasticity dynamics in ensembles of CA1 hippocampal pyramidal cells, which encode representations and memories of space and life experiences (Burgess et al., 2002; Buzsáki and Moser, 2013; Eichenbaum, 2004; Squire and Zola-Morgan, 1991). Past work has shown that hippocampal spatial representations have both dynamic and stable facets. In rodents that repeatedly visit a familiar environment, there is day-to-day turnover in the set of CA1 pyramidal cells representing this environment, which helps distinguish the representations of the different visits (Mankin et al., 2012; Ziv et al., 2013). Nevertheless, individual CA1 neural place fields can exhibit long-term stability (Lever et al., 2002), and repeated visits to an environment can selectively stabilize place fields of cells active during the first visit (Karlsson and Frank, 2008). However, ensemble patterns of hippocampal plasticity over long time periods remain unexplored. We tracked these patterns in area CA1 and assessed whether they stabilize over time, as in motor cortex (Cao et al., 2015), or continuously turn over, as do CA1 ensemble neural codes (Mankin et al., 2012; Ziv et al., 2013).

To track activity-evoked plasticity, we combined time-lapse *in vivo* two-photon microscopy, a chronic mouse preparation for repeated imaging of area CA1 (Attardo et al., 2015; Dombeck et al., 2010; Mizrahi et al., 2004), and a fluorescent reporter based on the promoter IEG *Arc* (also known as *Arc/Arg* 3.1). *Arc* has key roles in neural synaptic and cellular plasticity and is transiently activated after electrical excitation (Bramham et al., 2008; Shepherd and Bear, 2011). We used an enhanced form of the synaptic activity-responsive element (E-SARE) within the *Arc* enhancer/promoter region to drive a fluorescent reporter of IEG activity (Kawashima et al., 2009, 2013). Like *Arc*, E-SARE is rapidly activated by synaptic activity but has low basal expression otherwise, and the two have ~80% concordance in their

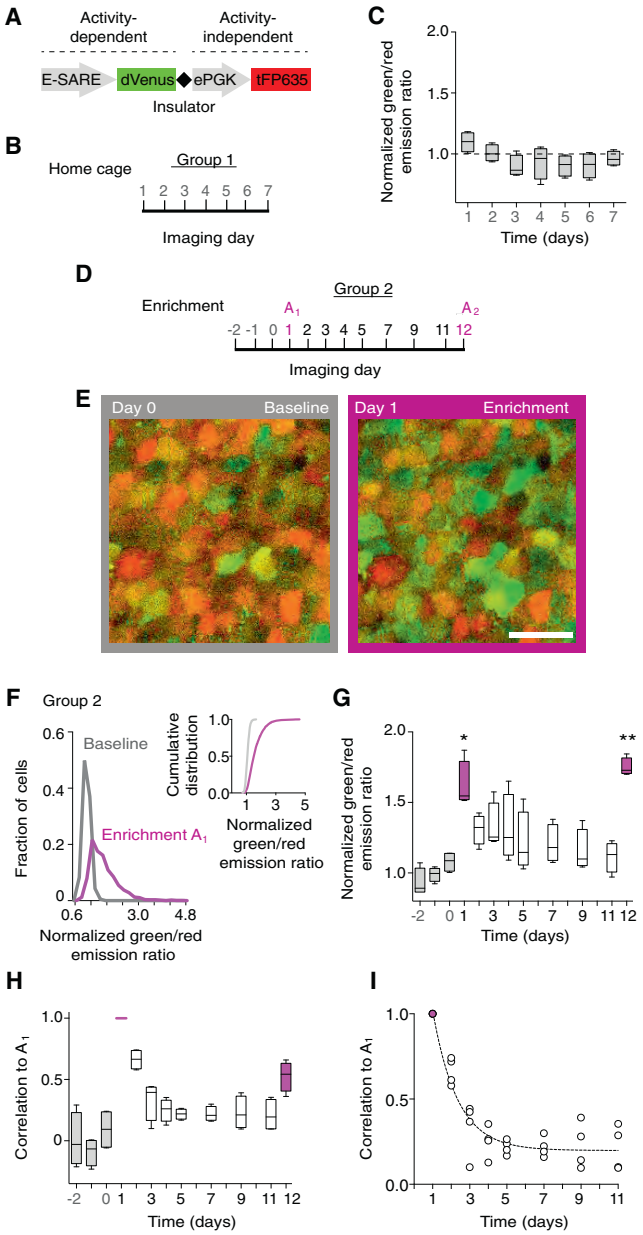

Figure 1. E-SARE Activation after Exploration of Enriched Environments

(A) To track E-SARE activation in CA1 pyramidal cells, we injected a virus from which E-SARE drove dVenus expression and the ePGK housekeeping promoter drove TurboFP635 expression.

(B) Timeline of sessions for group 1 (four mice, 12–14 weeks old, 461 ± 103 [SD] cells per mouse, range 344–557557 cells, 1,845 cells total).

(C) CA1 neurons' green/red emission ratios for group 1 mice, relative to each cell's mean ratio over days 1–3 of imaging (dashed line). Values were stationary across days 1–7 ($p = 0.27$, Friedman ANOVA; $n = 4$ mice).

(D) Timeline of sessions for group 2 (four mice, 12–14 weeks old, 330 ± 168 [SD] cells per mouse, 1,322 cells total). On days 1 and 12 (magenta), mice visited an EE for 2 hr. Other days, mice were in home cages.

(E) Two-photon images from a live mouse, showing the same cells on day 0 and after visiting an EE on day 1. Green, dVenus fluorescence; red, TurboFP635 fluorescence. Scale bar, 20 μm.

(F) Distributions of cells' green/red emission ratios shifted to larger values after mice visited an EE (magenta curve; day 1) compared with baseline days (gray curve; day 0) ($p < 0.0001$, Wilcoxon signed-rank test; $n = 1,322$ cells from four mice). Inset: the corresponding cumulative distributions highlight the change ($p < 0.00001$, Kolmogorov-Smirnov test).

(G) Box-and-whisker plot for group 2 mice of cells' green/red emission ratios, normalized to baseline values from days –2 to 0. Values are the mean ratios in each mouse and were higher on days when mice visited the EE (*$p = 0.015$ and **$p = 0.002$, Friedman ANOVA, Dunn's correction for multiple comparisons with day 0; $n = 4$ mice).

(H) Spearman correlation coefficients determined by comparing ensemble patterns of E-SARE activation with the pattern on day 1 (A_1). After A_1, these coefficients declined to a plateau, but the A_2 visit on day 12 evoked E-SARE patterns resembling those on day 1.

(I) The decline of correlation coefficients was well fit (dashed line) by an exponential decay ($r = 0.94$; time constant [τ_1] = 1.3 days).

In this and all figures, whiskers in box-and-whisker plots span a distribution's full range, boxes enclose the middle 50%, and horizontal lines denote median values. See also Figure S1 and Table S1.

expression patterns (Kawashima et al., 2013). Neurons in which E-SARE has been activated show, on average, greater electrical excitability but not higher rates of spontaneous activity, consistent with E-SARE's acting as a reporter of the plastic changes set in action along with *Arc* induction (Kawashima et al., 2013). However, as a synthetic promoter, E-SARE drives activity-dependent gene expression more potently than *Arc* or other IEG promoters but with similar kinetics, enabling a superior reporter of IEG activity (Kawashima et al., 2013).

We tracked E-SARE activation in thousands of CA1 cells over weeks as mice repeatedly explored different enriched environments (EEs). The cell ensemble activation patterns provided a characteristic representation of each environment. Patterns evoked by visits to the same environment on different days involved distinct but overlapping subsets of cells and grew increasingly similar over repeated visits. In mice performing a navigation task, the long-term dynamics of E-SARE activation closely resembled those after free exploration in the same spatial environment. Compared with young adults, E-SARE activation patterns in aged mice were less stable and provided less specific representations of space, which might play a role in spatial memory decline with age.

RESULTS

In Vivo Two-Photon Imaging of E-SARE Activation

To track E-SARE activation, we injected adult mice in the left dorsal CA1 hippocampal area with a viral vector expressing green fluorescent destabilized d2Venus via the E-SARE promoter and red fluorescent TurboFP635 via the ePGK promoter (Figure 1A; STAR Methods) (Kawashima et al., 2013). The ePGK promoter stably expressed TurboFP635, which provided a normalization factor to account for variations in viral particle numbers per cell and day-to-day changes in lighting or other imaging parameters. We tracked over days each cell's ratio of green to red fluorescence intensities as a metric of its E-SARE activation level, and we normalized these ratios to those observed in three baseline imaging sessions before the mice started behavioral assays.

For initial validation, we tracked baseline E-SARE activity by daily imaging of a set of control mice (group 1; Table S1) that

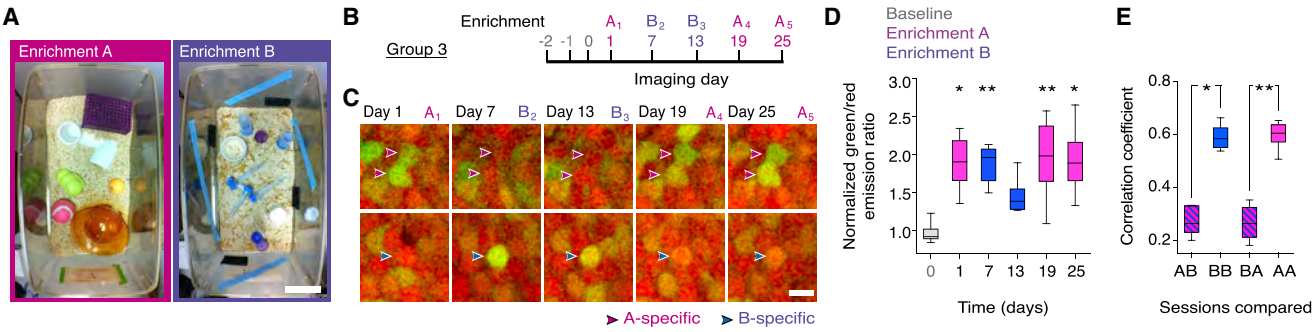

Figure 2. E-SARE Activation Patterns Represent Individual Environments

(A) Environments A and B for group 3 mice.

(B) Timeline of sessions for group 3 mice (six mice, 12–14 weeks old, 495 ± 57 [SD] cells imaged per mouse, 2,970 cells total).

(C) Maximum-intensity projections of two-photon image stacks acquired *in vivo* (four to six image slices per stack) showing E-SARE activation patterns specific for A and B. Green, dVenus fluorescence; red, TurboFP635 fluorescence.

(D) CA1 neurons' green/red emission ratios for group 3 mice, averaged for each mouse over all imaged cells and normalized to baseline values from days −2 to 0. Visits to A and B evoked rises in E-SARE activation (*p = 0.017 on days 1 and 25 and **p = 0.006 on days 7 and 19, Friedman ANOVA, Dunn's correction for multiple comparisons with day 0; n = 6 mice). Emission did not vary across explorations A_1, B_2, B_3, A_4, and A_5 (p = 0.23, Friedman ANOVA).

(E) Spearman correlation coefficients determined by comparing E-SARE activation patterns from successive sessions. Exposures to the same environment evoked patterns of significantly greater similarity than different environments (*p = 0.03 and **p = 0.007, Friedman ANOVA, Dunn's correction for multiple comparisons; n = 6 mice).

Scale bars, 10 cm (A) and 10 μm (C). See also Figure S1 and Table S1.

resided in their home cage (Figure 1B). Distributions of cells' baseline E-SARE activation levels were stationary over repeated sessions (Figure 1C). Separately, to assess the response of our fluorescent reporter system to a single behavioral episode, we monitored E-SARE activation for 72 hr after a single, 2 hr episode of free exploration in an environment enriched with novel objects, smells, and foods. This revealed that E-SARE activation peaked 6–8 hr after the episode's end (Figure S1A); thus in all subsequent studies we imaged mice 6–8 hr after the end of behavioral sessions. These data also showed that after a single evoked rise in d2Venus expression, intracellular concentrations of d2Venus decayed over the course of a few days, highlighting our method's limited ability to resolve rises in E-SARE activation spaced more closely in time than this. Consequently, we designed subsequent behavioral experiments such that successive behavioral sessions were generally multiple days apart.

Activation of E-SARE Is Transient and Repeatedly Evoked by Repeat Experiences

To probe the evolution of E-SARE activation following a single episodic experience, we allowed group 2 mice to visit an EE (A_1) for 2 hr and monitored E-SARE activation for 11 days afterward (Figures 1D and S1B). After exploration, cells' E-SARE levels rose above baseline (day 0) levels (Figures 1E and 1F). This rise did not recur on subsequent days when mice stayed in their home cages but did so upon a second visit (A_2) to the same environment on day 12 (Figure 1G).

Notably, the similarity of E-SARE activation patterns evoked by A_1 and those on subsequent days gradually declined, with kinetics well fit by an exponential decay (time constant [τ] = 1.3 days; Figures 1H and 1I). Despite similar levels of E-SARE activity, activation patterns evoked by A_1 and A_2, 12 days apart, were only modestly correlated (Figure 1H). Hence, two different visits, well separated in time, to the same environment can activate E-SARE to a comparable extent but with distinct patterns across the CA1 cell population.

Distinct Environments Evoke Distinct E-SARE Activation Patterns

To examine if E-SARE activation patterns are specific to individual environments, we imaged these patterns in mice (group 3) that repeatedly explored environments A and B over a 25 day period (Figures 2A and 2B). Given the ~1.3 day time for the decay in the similarity of evoked E-SARE patterns, we spaced the behavioral sessions 6 days apart to minimize crosstalk between measurements.

Environments A and B evoked comparable E-SARE levels, but many cells were activated by one environment but not the other (Figures 2C and 2D). The similarities of evoked E-SARE patterns were statistically indistinguishable between paired BB or AA visits (p = 0.84, Wilcoxon signed rank test; n = 6 mice), but these correlation coefficients were about twice as high as those for E-SARE patterns evoked by different environments (AB or BA) (Figure 2E). Overall, A and B each evoked distinguishable, robust expression patterns, showing the specificity of E-SARE activation patterns to an individual EE.

E-SARE Activation Patterns Are Specific to Individual Episodes

The moderate similarity between E-SARE activity patterns after two different visits to the same environment (Figure 1H) suggested that these patterns might exhibit turnover dynamics akin to those reported for CA1 representations of space on the basis of neural spiking or somatic Ca^{2+} activity (Mankin et al., 2012; Ziv et al., 2013). To characterize turnover, we imaged group 4 mice after each of six visits to the same environment (A_1–A_6) spaced over 1 month (Figures 3A–3D).

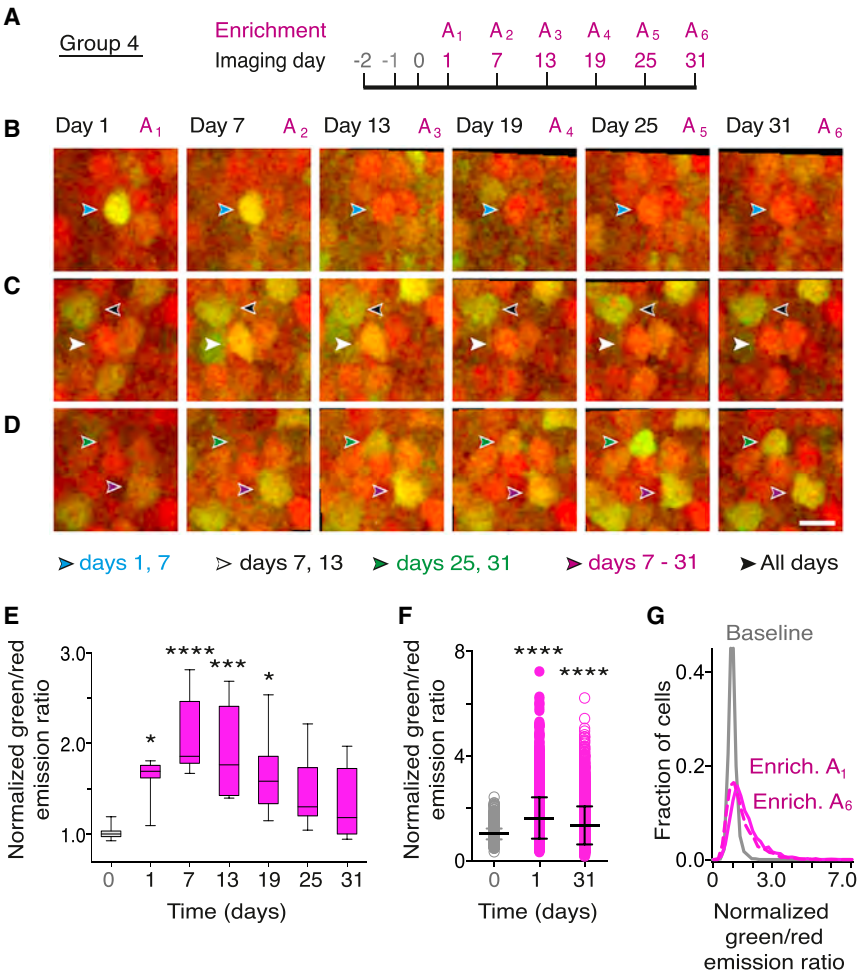

Figure 3. E-SARE Activation after Multiple Visits to One Environment

(A) Timeline of sessions for group 4 mice (eight mice, 12–14 weeks old, mean ± SD cells per mouse 455 ± 151, range 242–647 cells, total cells 3,642).

(B–D) Maximum-intensity projections of two-photon image stacks (four to six image slices per stack) show E-SARE patterns specific for different episodes. Example cells show E-SARE activation on 2 days (days 1 and 7, blue arrowheads, B; days 7 and 13, white arrowheads, C; days 25 and 31, green arrowheads, D), most days (days 7, 13, 25, and 31, magenta arrowheads, D), or all days (black arrowheads, B). Green, dVenus fluorescence; red, TurboFP635 fluorescence. Scale bar, 10 μm.

(E) Mean green/red fluorescence ratios of CA1 neurons in group 4 mice, normalized to baseline values from days −2 to 0. Initially, visits to A evoked significant rises in E-SARE activation over baseline levels (*$p < 0.05$, ***$p = 0.0003$, and ****$p < 0.0001$, Friedman ANOVA, Dunn's correction for multiple comparisons with day 0; n = 8 mice). Later on, evoked E-SARE expression levels returned to baseline.

(F) Green/red fluorescence ratios of individual neurons in group 4 mice reveal cells with higher E levels than baseline values in both the first and last imaging session (****$p < 0.0001$, Friedman ANOVA, Dunn's correction for multiple comparisons with day 0; n = 3,642 cells). Black data points denote mean ± SD.

(G) Distributions of cells' green/red ratios in group 4 mice shifted from baseline (gray curve, day 0) to larger values after behavioral sessions (solid magenta curve; day 1; dashed curve, day 31).

See also Figure S1 and Table S1.

All six visits plainly led to E-SARE activation, though median activation levels after the last two visits did not significantly exceed baseline values (Figure 3E). Nevertheless, at each time point there were subsets of cells with E-SARE levels up to 7 times baseline values (Figures 3F and 3G). Notably, some cells activated after all visits, but others activated after only some of the visits (Figures 3B–3D).

E-SARE Activation Patterns Stabilize over Multiple Visits to the Same EE

In group 4 mice we also examined the long-term dynamics of E-SARE activation patterns across the six visits to environment A. Declining correlations in E-SARE activity patterns after successive visits to A revealed episode-specific representations with decreasing similarity to the other representations of A as a function of the interval between visits (Figure 4A). This decline approached a non-zero plateau, indicative of long-term stability in the evoked activation pattern, with slower exponential kinetics (τ = 3.8 days) than those of group 1 mice that stayed in home cages (τ = 1.7 days; Figure 4B). Consistent with these results, the representations of A evolved faster earlier in the experimental timeline (Figure 4C), whereas E-SARE patterns across successive visits to A became highly correlated later in the timeline (median Spearman's $\rho = 0.71$ between the patterns evoked after A_5 and A_6), indicating a gradual stabilization of the patterns over a ~1 month interval; Figures 4D–4F and S1C). This stabilization depended upon the number of repeat exposures to environment A and was not simply due to the elapsed time (Figure S1D), as it did not occur to a significant extent in mice that stayed in their home cages for 1 week (group 1; Figure 4E), nor in mice that had the same experimental schedule but visited different environments (groups 3 and 5; Figures S1B and S1E–S1H).

The reduced levels of E-SARE activation across multiple visits to the same environment (Figure 3E) suggest that the rise in representational similarity (Figures 4D and S1C) may reflect at least two concurrent effects. First, some cells may have been active after initial but not later visits to A. Second, some cells may have become reliably activated after multiple visits.

To test for the first effect, we looked for cells that had high E-SARE expression initially but not after repeated visits to environment A. Over the month we tracked cells with the highest E-SARE expression levels (top 20% of all cells) after A_1. These cells had expression levels significantly higher than population mean levels only at early time points (Figure 4G), showing that

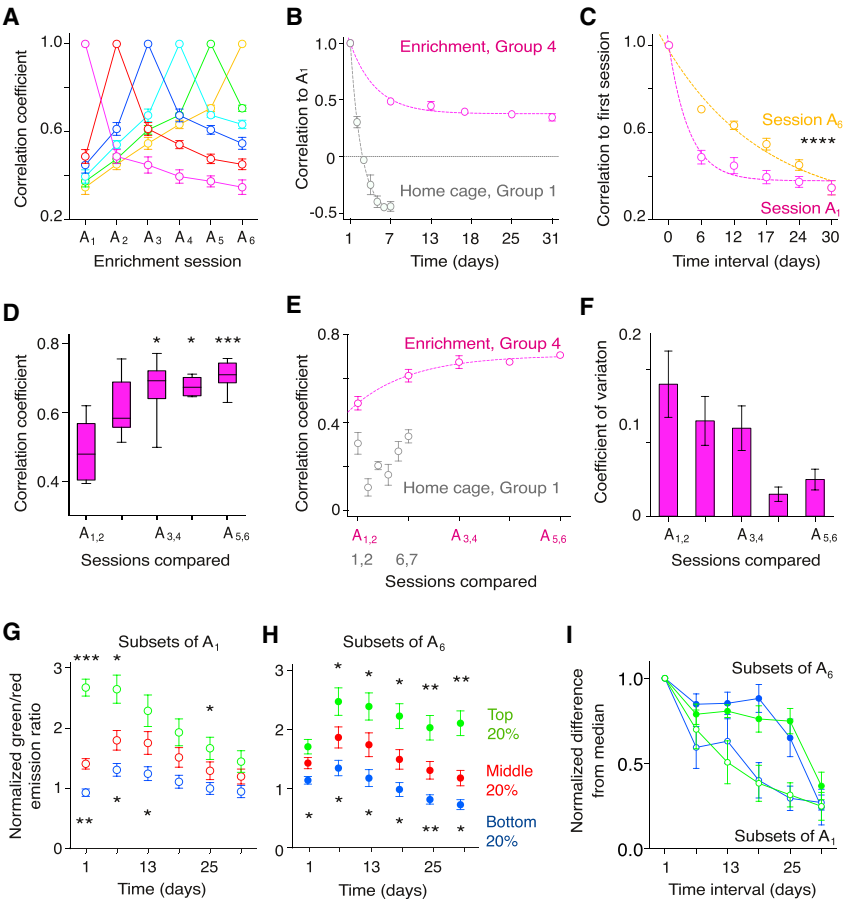

Figure 4. E-SARE Activation Patterns Stabilize after Multiple Visits to One Environment

(A) Mean ± SD Spearman correlation coefficients for group 4 mice comparing E-SARE activation patterns from each day to those on other days. Each color denotes a different reference day.

(B) Visits to A evoked E-SARE patterns whose correlations to that evoked on day 1 declined to a plateau and with slower kinetics (τ = 3.8 days) than those of mice who stayed in home cages (τ = 1.7 days). Dashed curves, exponential fits (****$p < 0.0001$, extra sum of squares F test comparing the fits).

(C) Mean ± SD Spearman correlation coefficients determined for group 4 mice by comparing E-SARE activation patterns evoked by A_1 (magenta) or A_6 (yellow) with those from other days separated by the intervals on the x axis. Comparisons with A_1 and A_6 patterns are plotted in opposite temporal order. Dashed curves, exponential fits. By ~4 days after A_1, E-SARE activation patterns lost similarity to that evoked by A_1 (τ = 3.8 days). Starting ~18 days before A_6, E-SARE activation patterns gained similarity to that evoked by A_6 (τ = 18.1 days). ****$p < 0.0001$, extra sum of squares F test comparing the exponential fits.

(D) Spearman correlation coefficients found by comparing E-SARE activation patterns after successive visits to environment A by group 4 mice. Values rose over repeated visits (*$p = 0.018$ and ***$p = 0.0003$, Friedman ANOVA, Dunn's correction for multiple comparisons with the $A_{1,2}$ correlation; n = 8 mice).

(E and F) In group 4 mice, evoked E-SARE activation patterns rose in similarity across successive sessions, as seen via increasing correlation coefficients between pairs of activation patterns (E) and declining coefficients of variation of the correlation coefficients (F) (computed from the distributions in (D). Group 1 mice lacked these effects. Dashed curve in (E), exponential fit (τ = 5.8 days).

(G and H) In each group 4 mouse, we sorted CA1 cells into quintiles according to their normalized green/red emission ratios, after the first visit (G) to A (day 1) or the last visit (day 31) (H) (mean ± SD cells per quintile per mouse 91 ± 30, range 49–129 cells). Plots show normalized ratios (mean ± SEM; eight mice) for the bottom (blue), middle (red), and top (green) quintiles. Fluorescence ratios for cells in the top and bottom quintile after visit A_1 (G) differed significantly from the population means only early in the timeline. Ratios for cells in the bottom quintile after A_6 (H) differed from the population means on all days, as did cells in the top quintile, except on the first day (*$p < 0.05$, **$p < 0.01$, and ***$p < 0.001$, Mann-Whitney U test comparing a quintile with population mean values at the same time point).

(I) We sorted cells into quintiles according to their green/red emission ratios after A_1 or A_6. We then calculated absolute differences between the median ratios of the top (green) and bottom (blue) quintiles and those of the whole cell population, and we normalized these differences to either their values on day 1 (for A_1 quintiles; open circles) or day 31 (for A_6 quintiles; closed circles). The plot shows the resulting mean ± SEM values (n = 8 mice), as a function of the time interval to the day on which the quintiles were defined. Consistent with a stabilization of E-SARE patterns, cells in the top and bottom quintiles after A_6 had green/red ratios more reliably distinct from population mean values than cells in top and bottom quintiles after A_1. Top and bottom quintiles defined on the A_6 data had distinct kinetics from those defined on A_1 data ($p < 0.0001$ for top A_1 versus top A_6 quintiles, $p = 0.0005$ for bottom A_1 versus A_6 quintiles, extra sum of squares F test to linear fits).

See also Table S1.

cells involved in the first representation of A were not necessarily involved in later representations. An analogous trend existed for cells with initially low E-SARE expression (bottom 20% of all cells after A_1; Figure 4G), showing that some cells absent from the first representation of A became involved later on after subsequent visits.

We next looked for a subset of cells that reliably activated on multiple occasions. If E-SARE expression patterns progressively stabilize, cells consistently expressing E-SARE should do so after A_6 and all or most of the prior explorations, $A_{1–5}$. To test this idea, we tracked cells within the top 20% of E-SARE expression levels after A_6 across all prior explorations ($A_{1–5}$). These cells had higher E-SARE levels than the population means at nearly all prior time points (Figure 4H). Hence, this subset of cells participated not only in the final, stabilized representation but also in the preceding representations of A. Similarly, cells with low E-SARE levels (bottom 20%; Figures 4H and 4I) after A_6 had consistently low expression at all prior time points and were not involved in any representation of A.

Overall, across repeated visits to the same environment, only a subset of cells that activated early on eventually contributed to the stabilized representation. Stabilized representations resulted

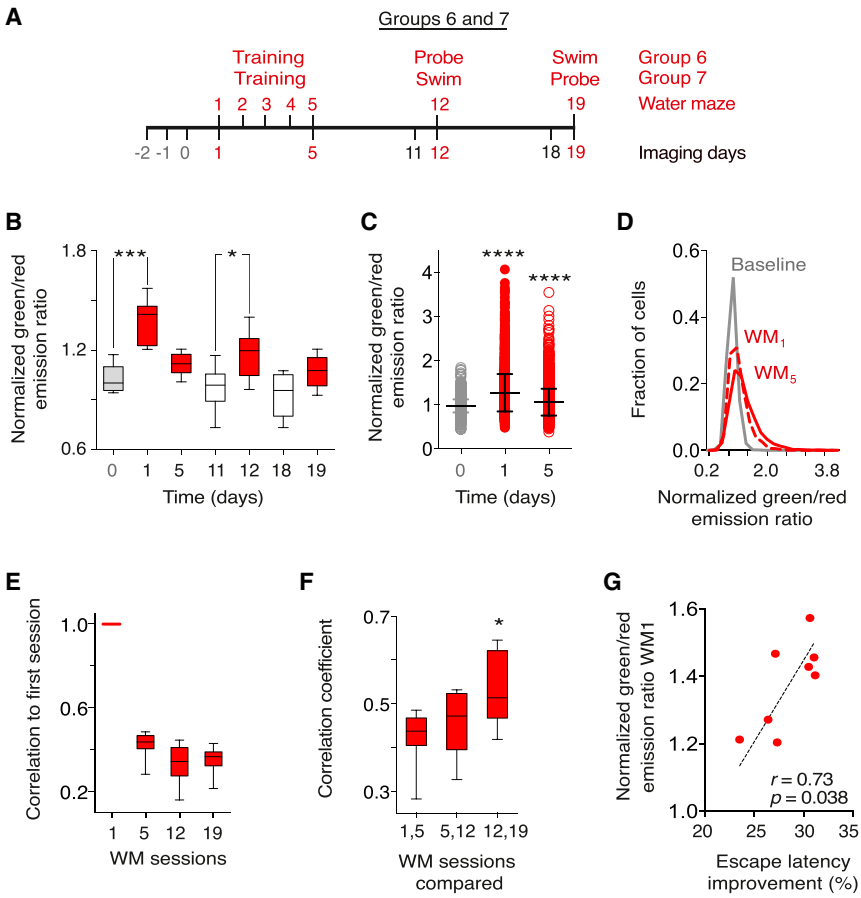

Figure 5. E-SARE Expression Patterns during Spatial Navigation and Recall

(A) Timeline of sessions for group 6 (four mice, 12–14 weeks old, 429 ± 243 [SD] cells per mouse, range 134–677 cells, 1,716 cells total) and group 7 mice (four mice, 425 ± 241 cells per mouse, range 121–727 cells, 1,702 cells total). All mice received water maze (WM) training on days 1–5 (5 min sessions). We tested their memory recall or had them swim to a visible platform (2 min WM session, days 12 and 19). Days marked in red involved the WM. We imaged mice at baseline (gray) and on two other days (black) when we took the mice directly from home cages to imaging.

(B) Mean green/red emission ratios for mice in groups 6 and 7, normalized to baseline values. E-SARE levels rose above baseline on days 1 and 12 *p = 0.011 and (***p = 0.0006, Friedman ANOVA, Dunn's correction for multiple comparisons with day 0 or 11; n = 8 mice).

(C) Green/red emission ratios for individual CA1 cells reveal cells with higher E-SARE levels after WM sessions than baseline values (****p < 0.0001, Friedman ANOVA, Dunn's correction for multiple comparisons with day 0; n = 3,995 cells). Black data points denote mean ± SD.

(D) Distributions of green/red emission ratios shifted to larger values after WM sessions (red curves; day 1, solid curve; day 5, dashed curve) compared with baseline days (gray curve, day 0).

(E) Spearman correlation coefficients comparing ensemble E-SARE activation patterns after each WM session with the pattern on day 1.

(F) Spearman correlation coefficients comparing ensemble E-SARE activation patterns after successive WM sessions. Correlation coefficients rose significantly over time (*p = 0.049, Friedman ANOVA, Dunn's correction for multiple comparisons with the first data point; n = 8 mice).

(G) Mean E-SARE activation levels in individual mice on the first day of WM training were predictive of subsequent improvements in WM performance during training. Each datum shows mean normalized E-SARE fluorescence levels in an individual mouse after its first exposure to the WM (day 1), plotted as a function of the mouse's improvement in escape latency on day 5.

Dashed line, linear fit. r and p values are Pearson correlation coefficients and significance values, respectively, for the linear regression. See also Figure S2 and Table S1.

from a gradual refinement in which plasticity patterns with progressively fewer cells grew increasingly similar to each other over repeated visits.

E-SARE Dynamics after Spatial Navigation or Free Exploration Are Similar

To examine whether a behavioral task requiring spatial memory formation and recall would influence E-SARE activity patterns, for 5 days we trained two groups of mice in a version of the Morris water maze (Morris, 1984) (Figure 5A; STAR Methods). Seven days after the end of training with a submerged platform, group 6 mice were tested for memory recall, whereas group 7 mice underwent a session of navigation to a visible platform (not requiring memory recall). Fourteen days after the end of training, group 7 mice were tested for memory recall and group 6 performed the navigation session (Figure S2A).

Both groups learned (Figure S2B) and recalled the platform location when tested 7 or 14 days after training (Figure S2C). In both groups, E-SARE activity levels and time courses were indistinguishable between memory recall and navigation sessions (Figures S2D–S2F), yielding no evidence that evoked E-SARE representations in CA1 were significantly influenced by the explicit behavioral requirement of memory use. Thus, we aggregated data from groups 6 and 7 for subsequent analyses.

The first water maze training session (day 1) led to a rise in mean E-SARE activation over baseline levels (day 0), but after five training sessions mean E-SARE levels returned to baseline (day 5; Figure 5B). Notwithstanding, a subset of cells maintained evoked E-SARE levels up to 4 times their baseline values (Figures 5C and 5D). Mean E-SARE levels again rose over baseline after the day 12 water maze session but to a lesser extent than at the start of training (Figure 5B).

Representations of water maze sessions turned over and significantly stabilized over time (Figures 5E and 5F). Mean E-SARE levels after the first water maze navigation predicted how well individual mice improved their navigation performance

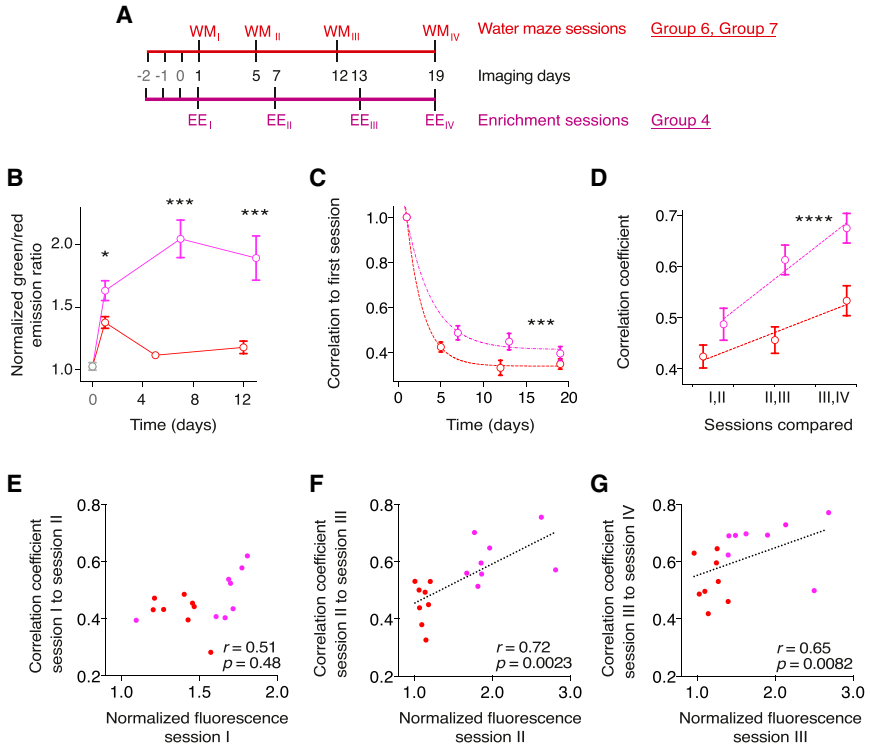

Figure 6. Free Exploration and a Spatial Navigation Task Evoke Similar Plasticity Dynamics

(A) Timeline of sessions for mice in groups 4, 6, and 7.

(B) Mean ± SEM green/red emission ratios for cells in group 4 (magenta points) and groups 6 and 7 (red points). Two to 5 min WM sessions evoked less E-SARE activation than 2 hr visits to EE (*p = 0.01 and ***p = 0.0002, Mann-Whitney U test comparing the two behaviors at each time point; n = 16 total mice).

(C) Mean ± SEM Spearman correlation coefficients determined by comparing E-SARE patterns after WM sessions (red, groups 6 and 7) or visits to environment A (magenta, group 4) to the pattern evoked on day 1. Coefficients declined exponentially with time (r values for groups 6 and 7 and group 4 were 0.97 and 0.95, respectively), with a faster decay for the WM (***p = 0.0004, extra sum of squares F test to the exponential fits).

(D) Mean ± SEM correlation coefficients between E-SARE patterns evoked by successive visits to WM (red, groups 6 and 7) or environment A (magenta, group 4). Correlations rose more slowly for groups 6 and 7 than for group 4 (****p < 0.0001, extra sum of squares F test to the linear fits).

(E–G) Correlation coefficients for evoked E-SARE patterns after successive sessions, as a function of the mean E-SARE level after the first session (E) in the pair for group 4 (magenta points) or groups 6 and 7 (red points) mice. There were significant relationships between mean E-SARE levels evoked by the second (F) or third (G) behavioral sessions and the similarity of the successive E-SARE pattern. Dashed lines, linear fits. r and p values are Pearson correlation coefficients and significance values, respectively, for the linear regressions.

See also Table S1.

over the 5 training days (Figure 5G), but the similarities of evoked E-SARE patterns of between the first and last days of training did not (Figure S2G). Neither E-SARE levels per se nor the similarities of E-SARE patterns predicted performance in the test sessions (Figures S2H and S2I).

A comparison of the water maze and enrichment groups (Figure 6A) showed that the latter had higher evoked E-SARE levels, slower turnover, and faster stabilization of the episode representations (Figures 6B–6D). However, with repeat experiences of either type, the E-SARE activation levels of each mouse became a good predictor of the similarity of the evoked representation to that of the next session (Figures 6E–6G).

Aging Reduces the Specificity and Stability of E-SARE Activation Patterns

We next studied how age-related differences in learning and memory affect ensemble E-SARE activation patterns. Aged mice reportedly have impairments in learning and memory (Bach et al., 1999), which we confirmed in the water maze task (Figures S3A–S3D).

We imaged E-SARE activation patterns in 23-month-old mice that visited two different (group 8) or a single EE (group 9) on the same schedule (Figure 7A). These visits evoked E-SARE levels above baseline (day 0) values, but in aged mice, baseline E-SARE levels were below those of young adults, largely because of a lack of cells with very high E-SARE activation (Figures 7B–7D). Given their lower baseline levels, aged mice had slightly greater evoked levels of E-SARE activity than young adults (relative to baseline in both groups; Figure 7E).

Unlike in young adult mice, in aged mice we found neither significant stabilization nor refinement of episodic representations (Figures 7F and S4A) nor subsets of cells that maintained across the experiment significantly higher or lower E-SARE levels than the population means (Figures S4B and S4C). However, the representations in aged mice had turnover kinetics that were statistically indistinguishable from those in young adults (Figure 7G).

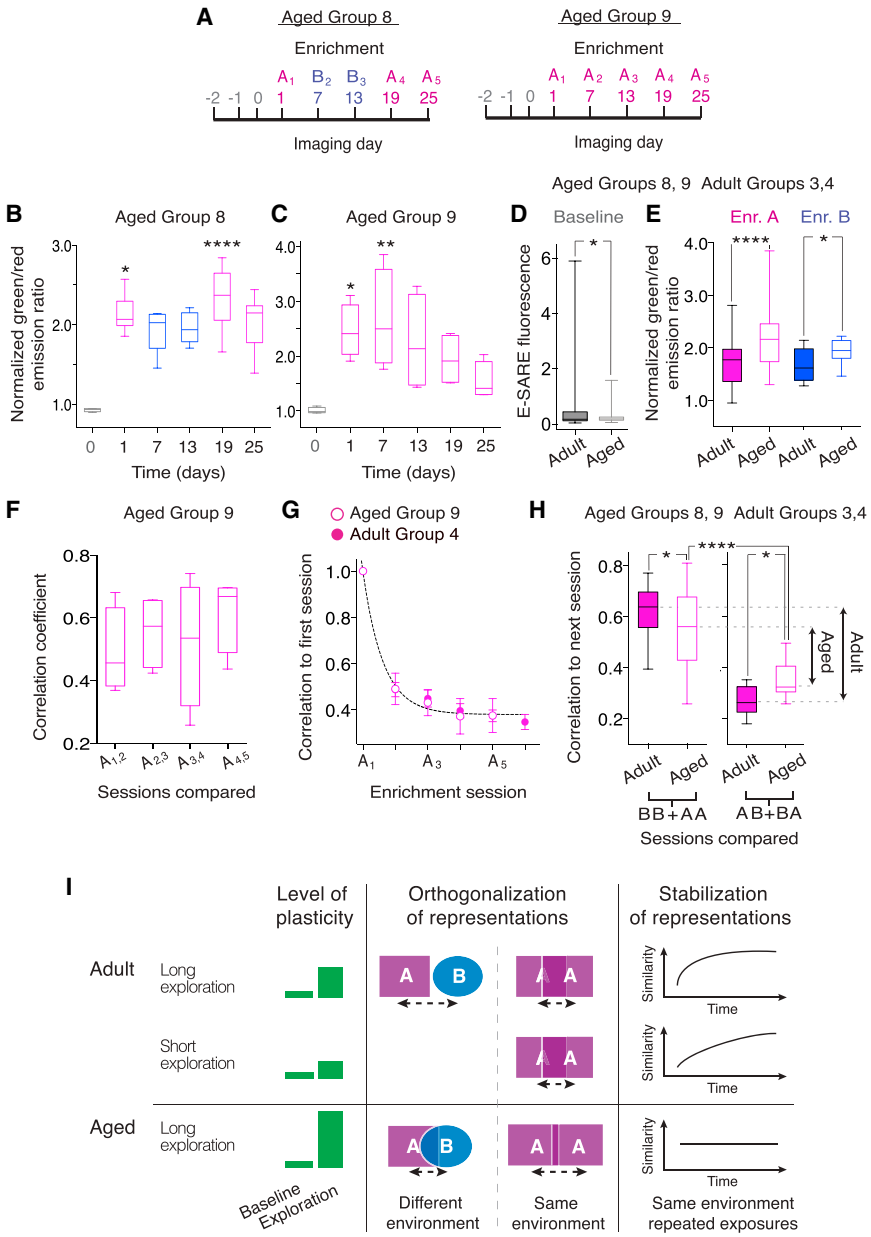

Figure 7. E-SARE Expression Patterns in Aged Mice Do Not Stabilize

(A) Timeline of sessions for group 8 (n = 6 mice, 23 months old, 256 ± 125 [SD] cells per mouse, range 122–471 cells, 1,538 cells total) and group 9 mice (n = 4 mice, 23 months old, mean ± SD 373 ± 118 cells per mouse, range 277–525 cells, 1,493 cells total).

(B and C) E-SARE activation in group 8 (B) and group 9 (C) mice relative to baseline levels (*p < 0.05, **p < 0.01, and ****p < 0.0001, Friedman ANOVA, Dunn's correction for multiple comparisons with day 0; six mice in B, four mice in C).

(D) Green/red emission ratios for all neurons imaged during the 3 day baseline period in aged or young adult mice. Young adults had higher E-SARE activity than aged mice (*p < 0.047, Mann-Whitney U test; n = 19,074 cells and 9,093 cells for young adults and aged mice, respectively).

(E) E-SARE levels after visits to environments A and B by aged or young adult mice, normalized to baseline values. Likely because of the lower baseline activation levels in aged mice (D), both environments induced modestly but significantly greater relative rises in E-SARE activation in aged mice (*p < 0.05 and ****p < 0.0001, Mann-Whitney U test; n = 114 visits to A, n = 24 visits to B).

(F) Spearman correlation coefficients determined by comparing patterns of E-SARE activation after successive visits to A by aged mice. Evoked E-SARE patterns did not increase in similarity over time (p = 0.24, Friedman ANOVA; n = 4 mice).

(G) Mean ± SEM Spearman correlation coefficients determined by comparing patterns of E-SARE activation with that on day 1. These coefficients had identical kinetics for aged and young adult mice (p = 0.9996, F test comparing exponential fits). Dashed line, exponential fit to the pooled data.

(H) Correlation coefficients for E-SARE activation patterns for pairs of visits to the same environment (BB and AA) or different environments (BA or AB). E-SARE patterns for successive visits to the same environment were less similar in aged mice than in young adults (*p = 0.03, Mann-Whitney U test; n = 70 total visits). Conversely, E-SARE patterns for visits to two different environments were more similar in aged mice than in young adults (*p = 0.021; n = 22 visits). Nevertheless, in aged mice, as in young adults, correlation coefficients were greater for visits to the same versus different environments (****p < 0.0001; n = 38 total visits), without difference between the BB and AA comparisons (p = 0.56, Wilcoxon signed rank test; n = 6 mice).

(I) Graphical summary of results. First column: levels of plasticity differ in young adults after long and short explorations of an EE or water maze and in aged animals after exploration of an EE. Second column: in aged mice, representations of two different environments are less distinct than in young adults, but representations of two different visits to the same environment are more distinct than in young adults. The overall effect is a reduction in each representation's distinctiveness in aged mice. Marked distances between icons indicate the similarity of representations for two different environments or two visits to the same environment. Third column: aged mice do not consolidate their plasticity representations. Representations in young adults consolidate faster after episodes of longer duration.

See also Figures S3 and S4 and Table S1.

In aged mice, different representations of the same environment were significantly more similar to one another than those of different environments, but this effect was more prominent in younger mice (Figures 7H and 7I). Conversely, representations of different environments were less similar to one another in young adult animals than in aged animals (Figures 7H and 7I). Furthermore, in aged mice, E-SARE levels did not predict the similarity of the evoked representation to that after the next visit, unlike in young adults (Figures S4D and S4E). Overall, it seems aging uncouples E-SARE activity levels from representational

specificity. Aged mice show lower baseline levels of E-SARE activity (Figure 7D) and hence slightly greater ratios of evoked E-SARE activity over baseline values (Figure 7E), but the patterning of this activation is less specific for individual environments and does not stabilize (Figures 7F, 7H, 7I, S4F, and S4G).

DISCUSSION

Deep-brain fluorescence imaging has allowed studies of structural plasticity (Attardo et al., 2015; Mizrahi et al., 2004) and Ca^{2+} activity (Dombeck et al., 2010; Ziv et al., 2013) in CA1 pyramidal cells. To study IEG activation in CA1 cell ensembles, we combined time-lapse two-photon imaging with a fluorescent reporter of synaptic activity-evoked IEG expression (Kawashima et al., 2013).

Unbiased Analyses of IEG Activity

Our approach has several advantages over prior methods for examining hippocampal plasticity. First, our dual cassette vector enables independent reporting of viral labeling and IEG activation, allowing evenhanded comparisons of different cells within and across different subjects. Second, time-lapse imaging allows longitudinal analyses of how individual cells respond over long time periods and to multiple behavioral experiences. Third, our analyses avoid classifying cells as ''active'' or ''inactive'' (Guzowski et al., 1999; Wang et al., 2006) but instead consider all imaged cells irrespective of fluorescence and E-SARE levels. Thus, the IEG representations we found involve not just cell identities but also their E-SARE activity levels, even in cells with weak E-SARE activity.

A caveat is that although E-SARE is designed to report *Arc* expression, the patterns and kinetics of gene expression driven from the two promoters do not fully agree (Kawashima et al., 2013). E-SARE expression levels do, however, reflect recent episodes of synaptically driven excitation (Kawashima et al., 2013). Downstream of any IEG, many factors influence the plasticity of neural electrical dynamics, to which all extant reporters of IEG transcription are impervious. Thus, how IEG activation affects neuronal electrophysiology remains poorly understood.

Experience-Dependent Refinement of CA1 Neural Ensembles

Given that Arc transcription is driven by synaptic activation, the turnover of cells activated by repeated similar experiences plausibly reflects the analogous turnover of place cells in the CA1 representation of space (Mankin et al., 2012; Ziv et al., 2013). The ~4 day decay time constant in the similarity of E-SARE activity patterns upon repeated visits to one environment is comparable with that of the similarity decline in CA1 representations determined by Ca^{2+} imaging in mice repeatedly visiting a familiar environment (Ziv et al., 2013). However, in mice re-visiting a familiar environment, the net number of active place neurons as detected by Ca^{2+} imaging remains constant (Ziv et al., 2013), whereas here we found that during the first few explorations of a novel environment, the number of cells in which E-SARE is activated gradually declines.

Notwithstanding this turnover, E-SARE activation patterns refined and stabilized across multiple repeat experiences (Figures 4 and 7I). This effect that was more prominent in mice that underwent enrichment sessions than in those that had water maze sessions, likely because of the different durations involved (2 hr enrichment versus 2–5 min water maze sessions). The stabilized patterns were specific to individual environments, consistent with the observation that different subsets of CA1 cells express *Arc* mRNA in different environments (Guzowski et al., 1999), which might help form invariant spatial representations. Over the stabilization process, E-SARE activity levels declined even while a subset of cells maintained activation levels 4–7 times baseline values. Cells that consistently had the highest E-SARE levels across repeated visits to an environment likely encoded environmental or episodic features common to or shared across the multiple experiences. These results are consistent with past studies in neocortex that reported similar phenomena (Cao et al., 2015; Wang et al., 2006; Xie et al., 2014).

Aged Mice Show Decreased Stability of IEG Activation Patterns

In dorsal CA1, aged mice have lower baseline levels of E-SARE activation than young adults, and thus aged mice show slightly greater behaviorally evoked rises in E-SARE activation over baseline values (Figure 7). Past studies comparing *Arc* mRNA levels in aged versus young adult rats were insensitive to differences in baseline levels of *Arc* expression and did not report this effect (Small et al., 2004). Strikingly, ensemble patterns of E-SARE activation in aged mice did not stabilize and were not as specific to particular environments as in young adults (Figures 7F, 7H, and 7I), consistent with electrical recordings of hippocampal place cell activity in rats (Barnes et al., 1997).

Prior work has shown that increasing the excitability of a sparse population of CA1 pyramidal cells in aged mice can improve their ability to link memories of distinct episodes (Cai et al., 2016). It would be interesting to test whether increasing the overall excitability of CA1 in aged mice might help restore the stabilization and specificity of IEG representations and thereby mitigate age-related memory deficits. More generally, it remains to be tested whether age-related changes in the long-term dynamics of IEG expression seen here are a bona fide cause of impaired learning and memory and not just a correlate.

Relationships of E-SARE Activation to Learning and Long-Term Memory

Hippocampal representations have two characteristics that, at first blush, might seem contradictory. On one hand, cell ensemble representations gradually refine and stabilize over the course of multiple similar episodes, which might enable invariant long-term representations (Karlsson and Frank, 2008; Mizuseki and Buzsáki, 2013). These representations are specific to individual environments, as found here and by ensemble neural Ca^{2+} imaging (Cai et al., 2016; Rubin et al., 2015). On the other hand, these representations exhibit ongoing cellular turnover, which might endow long-term memories with a unique time stamp, distinguishing similar experiences far apart in time or binding distinct experiences occurring in temporal proximity (Cai et al., 2016; Leutgeb et al., 2005; Manns et al., 2007; Rubin et al., 2015; Ziv et al., 2013). The opponent requirements for

cellular stabilization and turnover might support lifelong needs for continuous learning and the ability to link multiple experiences together. Our study is the first to monitor longitudinally these two facets of hippocampal representations at the level of neural ensemble IEG dynamics, and it thereby sets the stage for direct comparisons and causal manipulations of the relationships between long-term IEG dynamics and memory performance.

Several facets of our observational data are consistent with the purported role for IEG activation in learning and memory. Over repeated visits to the same environment, mean E-SARE levels across the cell population declined, suggesting that novelty might be needed for widespread E-SARE expression. The refinement, stabilization, and repeated activation of a subset of cells with E-SARE activation levels 4–7 times baseline levels are all consistent with a role for this subset in memory formation and consolidation. In water maze experiments, E-SARE activity at the start of training was also predictive of a mouse's performance improvement across the 5 training days.

Other aspects of our results are more puzzling. In the water maze, E-SARE dynamics after memory recall sessions were statistically indistinguishable from those after swim sessions. During swim sessions, even though the mice were not scored for their memory recall, they probably still experienced memories of prior episodes in the maze, which might account for the similar E-SARE dynamics. Moreover, we found no significant relationships between E-SARE dynamics in individual mice during water maze training and their memory performance as subsequently tested 7 or 14 days after the end of training. We suspect that this is due to the statistically significant but modest levels of memory that mice exhibit in the water maze test with a gap of 1–2 weeks after their last training session, which makes it statistically challenging to identify factors that significantly correlate with the behavioral performance of individual animals. In comparison, a contextual fear conditioning study in which memory testing was performed 2 d after training reported strong correlations between memory performance and the degree to which cells activated during trained underwent re-activation during memory testing, as assessed using the *c-Fos* IEG (Tanaka et al., 2014). The differences between this past result and ours may be due to the distinct properties of the two IEGs (Fos versus E-SARE), the greater saliency of a fear memory, and the different intervals between memory training and testing.

Many questions remain about the role of IEG activation in the plasticity of hippocampal neural ensembles, as the cellular events and transformations that encode spatial representations and long-term memories remain obscure. The relative contributions of online neural activity and offline re-play during sleep (Diekelmann and Born, 2010) to the refinement of plasticity patterns also remain undetermined. If sparse, long-lasting neural representations are important for long-term hippocampal memory, what are the cellular changes that neurons recruited into this representation undergo, and how do these changes support long-term memory? What mechanisms set the timescale of turnover of cells into and out of hippocampal representations? To address these questions and reveal the relationships among ensemble IEG plasticity, hippocampal memory, and its decline during aging, researchers should combine long-term imaging of neural activity in behaving animals with methods for monitoring and manipulating plasticity dynamics.

STAR★METHODS

Detailed methods are provided in the online version of this paper and include the following:

- KEY RESOURCES TABLE
- CONTACT FOR REAGENT AND RESOURCE SHARING
- EXPERIMENTAL MODELS AND SUBJECT DETAILS
  - Mice
- METHOD DETAILS
  - Virus
  - Surgery
  - *In vivo* two-photon microscopy
  - Navigation of EEs
  - Morris water maze
- QUANTIFICATION AND STATISTICAL ANALYSIS
  - Image and data analysis
- DATA AND SOFTWARE AVAILABILITY

SUPPLEMENTAL INFORMATION

Supplemental Information includes four figures and one table and can be found with this article online at https://doi.org/10.1016/j.celrep.2018.09.064.

ACKNOWLEDGMENTS

We thank J. Li, Y. Kondo, and M. Okamura for technical assistance. Drs. M. Shamloo and M. Lasnier of the Stanford Behavioral and Functional Neuroscience Laboratory oversaw and performed the water maze assays. We appreciate grants from the NIH (M.J.S.), the Ellison Foundation (M.J.S.), CREST-AMED (H.B.), Brain/MINDS (H.B.), the Takeda Science Foundation (H.B.), KAKENHI (15H02358, 17K19442, and 17H06312 to H.B. and 15H04258 to H.O.), and the Max Planck Society (A.A.) and fellowships from the National Science Foundation (J.E.F.), Stanford University (J.E.F.), and the Japan Society for the Promotion of Science (T.K.).

AUTHOR CONTRIBUTIONS

A.A. conducted and analyzed experiments. J.L. and J.E.F. contributed to the analyses. T.K., H.O., and H.B. designed and validated E-SARE reporter and the viral vector. A.A. and M.J.S. designed experiments and wrote the manuscript. M.J.S. and H.B. supervised the project.

DECLARATION OF INTERESTS

The authors declare no competing interests.

Received: March 30, 2017
Revised: June 27, 2018
Accepted: September 19, 2018
Published: October 16, 2018

REFERENCES

Attardo, A., Fitzgerald, J.E., and Schnitzer, M.J. (2015). Impermanence of dendritic spines in live adult CA1 hippocampus. Nature *523*, 592–596.

Bach, M.E., Barad, M., Son, H., Zhuo, M., Lu, Y.F., Shih, R., Mansuy, I., Hawkins, R.D., and Kandel, E.R. (1999). Age-related defects in spatial memory are correlated with defects in the late phase of hippocampal long-term

potentiation in vitro and are attenuated by drugs that enhance the cAMP signaling pathway. Proc. Natl. Acad. Sci. U S A *96*, 5280–5285.

Bailey, C.H., and Kandel, E.R. (1993). Structural changes accompanying memory storage. Annu. Rev. Physiol. *55*, 397–426.

Barnes, C.A., Suster, M.S., Shen, J., and McNaughton, B.L. (1997). Multistability of cognitive maps in the hippocampus of old rats. Nature *388*, 272–275.

Bramham, C.R., Worley, P.F., Moore, M.J., and Guzowski, J.F. (2008). The immediate early gene arc/arg3.1: regulation, mechanisms, and function. J. Neurosci. *28*, 11760–11767.

Burgess, N., Maguire, E.A., and O'Keefe, J. (2002). The human hippocampus and spatial and episodic memory. Neuron *35*, 625–641.

Buzsáki, G., and Moser, E.I. (2013). Memory, navigation and theta rhythm in the hippocampal-entorhinal system. Nat. Neurosci. *16*, 130–138.

Cai, D.J., Aharoni, D., Shuman, T., Shobe, J., Biane, J., Song, W., Wei, B., Veshkini, M., La-Vu, M., Lou, J., et al. (2016). A shared neural ensemble links distinct contextual memories encoded close in time. Nature *534*, 115–118.

Cao, V.Y., Ye, Y., Mastwal, S., Ren, M., Coon, M., Liu, Q., Costa, R.M., and Wang, K.H. (2015). Motor learning consolidates Arc-expressing neuronal ensembles in secondary motor cortex. Neuron *86*, 1385–1392.

Caroni, P., Donato, F., and Muller, D. (2012). Structural plasticity upon learning: regulation and functions. Nat. Rev. Neurosci. *13*, 478–490.

Diekelmann, S., and Born, J. (2010). The memory function of sleep. Nat. Rev. Neurosci. *11*, 114–126.

Dombeck, D.A., Harvey, C.D., Tian, L., Looger, L.L., and Tank, D.W. (2010). Functional imaging of hippocampal place cells at cellular resolution during virtual navigation. Nat. Neurosci. *13*, 1433–1440.

Eichenbaum, H. (2004). Hippocampus: cognitive processes and neural representations that underlie declarative memory. Neuron *44*, 109–120.

Guzowski, J.F., McNaughton, B.L., Barnes, C.A., and Worley, P.F. (1999). Environment-specific expression of the immediate-early gene Arc in hippocampal neuronal ensembles. Nat. Neurosci. *2*, 1120–1124.

Karlsson, M.P., and Frank, L.M. (2008). Network dynamics underlying the formation of sparse, informative representations in the hippocampus. J. Neurosci. *28*, 14271–14281.

Kawashima, T., Okuno, H., Nonaka, M., Adachi-Morishima, A., Kyo, N., Okamura, M., Takemoto-Kimura, S., Worley, P.F., and Bito, H. (2009). Synaptic activity-responsive element in the Arc/Arg3.1 promoter essential for synapse-to-nucleus signaling in activated neurons. Proc. Natl. Acad. Sci. U S A *106*, 316–321.

Kawashima, T., Kitamura, K., Suzuki, K., Nonaka, M., Kamijo, S., Takemoto-Kimura, S., Kano, M., Okuno, H., Ohki, K., and Bito, H. (2013). Functional labeling of neurons and their projections using the synthetic activity-dependent promoter E-SARE. Nat. Methods *10*, 889–895.

Leslie, J.H., and Nedivi, E. (2011). Activity-regulated genes as mediators of neural circuit plasticity. Prog. Neurobiol. *94*, 223–237.

Leutgeb, S., Leutgeb, J.K., Barnes, C.A., Moser, E.I., McNaughton, B.L., and Moser, M.-B. (2005). Independent codes for spatial and episodic memory in hippocampal neuronal ensembles. Science *309*, 619–623.

Lever, C., Wills, T., Cacucci, F., Burgess, N., and O'Keefe, J. (2002). Long-term plasticity in hippocampal place-cell representation of environmental geometry. Nature *416*, 90–94.

Mankin, E.A., Sparks, F.T., Slayyeh, B., Sutherland, R.J., Leutgeb, S., and Leutgeb, J.K. (2012). Neuronal code for extended time in the hippocampus. Proc. Natl. Acad. Sci. U S A *109*, 19462–19467.

Manns, J.R., Howard, M.W., and Eichenbaum, H. (2007). Gradual changes in hippocampal activity support remembering the order of events. Neuron *56*, 530–540.

Mizrahi, A., Crowley, J.C., Shtoyerman, E., and Katz, L.C. (2004). High-resolution in vivo imaging of hippocampal dendrites and spines. J. Neurosci. *24*, 3147–3151.

Mizuseki, K., and Buzsáki, G. (2013). Preconfigured, skewed distribution of firing rates in the hippocampus and entorhinal cortex. Cell Rep. *4*, 1010–1021.

Morris, R. (1984). Developments of a water-maze procedure for studying spatial learning in the rat. J. Neurosci. Methods *11*, 47–60.

Rogerson, T., Cai, D.J., Frank, A., Sano, Y., Shobe, J., Lopez-Aranda, M.F., and Silva, A.J. (2014). Synaptic tagging during memory allocation. Nat. Rev. Neurosci. *15*, 157–169.

Rubin, A., Geva, N., Sheintuch, L., and Ziv, Y. (2015). Hippocampal ensemble dynamics timestamp events in long-term memory. eLife *4*, 723.

Shepherd, J.D., and Bear, M.F. (2011). New views of Arc, a master regulator of synaptic plasticity. Nat. Neurosci. *14*, 279–284.

Small, S.A., Chawla, M.K., Buonocore, M., Rapp, P.R., and Barnes, C.A. (2004). Imaging correlates of brain function in monkeys and rats isolates a hippocampal subregion differentially vulnerable to aging. Proc. Natl. Acad. Sci. U S A *101*, 7181–7186.

Squire, L.R., and Zola-Morgan, S. (1991). The medial temporal lobe memory system. Science *253*, 1380–1386.

Tanaka, K.Z., Pevzner, A., Hamidi, A.B., Nakazawa, Y., Graham, J., and Wiltgen, B.J. (2014). Cortical representations are reinstated by the hippocampus during memory retrieval. Neuron *84*, 347–354.

Wang, K.H., Majewska, A., Schummers, J., Farley, B., Hu, C., Sur, M., and Tonegawa, S. (2006). In vivo two-photon imaging reveals a role of arc in enhancing orientation specificity in visual cortex. Cell *126*, 389–402.

West, A.E., and Greenberg, M.E. (2011). Neuronal activity-regulated gene transcription in synapse development and cognitive function. Cold Spring Harb. Perspect. Biol. *3*, a005744.

Xie, H., Liu, Y., Zhu, Y., Ding, X., Yang, Y., and Guan, J.S. (2014). In vivo imaging of immediate early gene expression reveals layer-specific memory traces in the mammalian brain. Proc. Natl. Acad. Sci. U S A *111*, 2788–2793.

Ziv, Y., Burns, L.D., Cocker, E.D., Hamel, E.O., Ghosh, K.K., Kitch, L.J., El Gamal, A., and Schnitzer, M.J. (2013). Long-term dynamics of CA1 hippocampal place codes. Nat. Neurosci. *16*, 264–266.

STAR★METHODS

KEY RESOURCES TABLE

REAGENT or RESOURCE	SOURCE	IDENTIFIER
Bacterial and Virus Strains		
AAV2/1-ITR-E-SARE-d2Venus-pA-cHS4-ePGK-TurboFP635-WPRE-pA-ITR	Haruhiko Bito (Kawashima et al., 2013)	N/A
Experimental Models: Organisms/Strains		
Mouse: WT C57Bl6	Jackson Laboratory	#000664
Software and Algorithms		
Data analysis: MATLAB	Mathworks	Mathworks.com
Data analysis: Prism	Graphpad	Graphpad.com
Image acquisition: Prairie View	Prairie	Bruker.com
Behavioral tracking: Ethovision	Noldus	Noldus.com
Other		
Two-photon microscope: Prairie Ultima	Prairie	Bruker.com
Titanium-sapphire laser: Chameleon Ultra II	Coherent	Coherent.com
Water Maze: circular water tank (1.8 m diameter, 0.6 m in depth)	Custom made	N/A

CONTACT FOR REAGENT AND RESOURCE SHARING

Further information and requests for resources and reagents should be directed to and will be fulfilled by the Lead Contact, Mark J. Schnitzer (mschnitz@stanford.edu)

EXPERIMENTAL MODELS AND SUBJECT DETAILS

Mice

We used wild-type C57Bl6 male mice, 12–14 week or 23 mo in age at the start of imaging. The Stanford Administrative Panel on Laboratory Animal Care approved all procedures.

METHOD DETAILS

Virus

We used an adeno-associated viral vector (AAV2/1-ITR-E-SARE-d2Venus-pA-cHS4-ePGK-TurboFP635-WPRE-pA-ITR) ($\sim 10^{13}$ viral particles/mL) expressing the E-SARE-d2Venus-insulator-ePGK-TurboFP635-WPRE reporter of activity-evoked neural plasticity (Kawashima et al., 2013).

Surgery

We anesthetized mice with isoflurane (2.5%–1.5% in O_2) and placed them in a stereotactic apparatus. We made a scalp incision, removed the periosteum and drilled two holes ($\sim$0.7 mm diameter) in the left hemisphere (1.8 mm and 2.8 mm posterior to bregma, 1.4 mm and 2.0 lateral to midline, respectively). Using a micro-pump and a 36G beveled metal needle, we delivered 0.5 μL viral suspension through each of the two holes, at depths of 1.6 mm and 1.8 mm ventral to bregma, respectively.

Two weeks later we implanted an imaging cannula just dorsal to area CA1. The cannula was a glass capillary (2.0-mm-ID; 2.4-mm-OD; 2 mm in length) sealed on one end with a 2.4-mm-diameter, #0 coverslip. After anesthesia and head fixation we removed scalp and periosteum and implanted a stainless steel screw in the right hemisphere of the cranium (2.0 mm posterior to bregma; 1.6 mm lateral to midline). We made a craniotomy (2.4 mm diameter) in the left hemisphere (2.0 ± 0.3 mm posterior to bregma; 2.0 ± 0.3 mm lateral to midline). Under visual guidance using a low-magnification stereoscope, we applied gentle suction to remove cortical tissue until we reached corpus callosum. After bleeding resolved, we lowered the cannula to be just dorsal to CA1. We covered the exposed skull and portion of the cannula protruding from the cranium with dental acrylic cement. After intraperitoneal administration of buprenorphine (Buprenex; 0.1 mg/kg) and carprofen (Rimadyl; 5-10 mg/kg), we transferred mice to a recovery cage, observed them until they awoke, and returned them to the home cages. Two-photon imaging began two weeks after cannula implantation.

In vivo two-photon microscopy

We used a two-photon microscope (Prairie Technologies) equipped with an ultrafast Ti:Sapphire laser (Chameleon II, Coherent) tuned to emit 920-nm light, which excited both TurboFP635 and dVenus. We performed dual-color detection using a dichroic mirror (Semrock FF560-di01 = 25x36) to separate green and red fluorescence, two distinct emission filters (Semrock FF01-630/92-25 and FF01-525/40-25), a pair of photomultiplier tubes, and a water immersion objective lens (Olympus LUMPlan FI/IR 0.8 NA 40 ×).

Each mouse underwent four days of handling and habituation to the imaging setup, and then three sessions of baseline imaging. We imaged anesthetized mice (1.5% isoflurane in O_2) for a total of 8–12 sessions (each 60–90 min long) using ~5–20 mW illumination at the sample plane.

In each mouse's first imaging session, we chose several areas of brain tissue (1–9 per mouse) for longitudinal monitoring. We acquired dual color image stacks of these volumes (approximately 300 × 300 × 200 μm^3; voxel size: 0.58 × 0.58 × 3 μm^3).

Navigation of EEs

EEs were created in cages larger [42(l) × 21.5(w) × 21.5(h) cm^3] than standard home cages with unique sets of objects, foods and smells. Such objects included running wheels, plastic tunnels, and objects of various colors, textures and shapes, and foods of distinct flavors. EEs all had the same bedding, which was distinct from home cage bedding. Each environment resided in a different laboratory room. Mice freely explored each environment in 2 h sessions, during which we provided food and water *ad libitum*.

Morris water maze

We trained mice in a variant of the classic maze (Morris, 1984) in which they learned to swim to a platform submerged in milky-colored water in a circular arena. Mice performed daily training sessions for 5–7 d (five trials, each 1 min long, per session). We released mice at random locations and allowed them to swim to the platform. If they did not find the platform within 1 min, we manually placed them on the platform for 10 s. We defined escape latency as the elapsed time until mounting of the submerged platform. We defined improvement in escape latency as the difference between escape latencies on the first and last day of WM training, normalized by the sum of the latencies on all training days.

Mice received one or two probe sessions (two 1-min-trials per session) in the same arena but without the platform. In these sessions the target quadrant was the one where the platform had been during training. We defined the normalized quadrant time (Figures S2C and S3C,D) as the total time a mouse spent in a specific quadrant, divided by the mean time spent in the three non-target quadrants. Some mice received a swim session (two 1-min-trials per session), during which they had to swim to a visible platform located in a position different than that of the training platform. In all cases, we imaged E-SARE levels 6–8 h after the end of the behavioral session.

QUANTIFICATION AND STATISTICAL ANALYSIS

Image and data analysis

We used custom software written in MATLAB to register image stacks acquired at the same tissue sites at distinct time points. To align the stacks, we chose at least 10 cell bodies that were stable across the time series and used rigid image alignment to minimize displacements of cell body centroids over time.

To score the brightness values of each cell over the time series, we opened the data at a random time point (the experimenter was blind to the time point used), selected a cell body, and drew a circular region-of-interest (ROI) ~4.64 μm in diameter, smaller than a neural cell body. After centering the ROI on the cell at the tissue depth at which the soma's lateral width was broadest, we recorded mean TurboFP635 and Venus fluorescence values averaged over all pixels in the ROI. We then progressed to the next time point, scored the cell in the same way, and iterated this procedure for all time points and all visible cells in the longitudinal dataset.

To account for variations in fluorophore expression and illumination fluctuations, we normalized the mean value of each neuron's (activity-dependent) dVenus emission by its mean (activity-independent) TurboFP635 emission. To monitor each cell's time-dependent level of E-SARE activation, we tracked its normalized (green divided by red) fluorescence values relative to those during the 3-d-baseline period. To assess the similarity of ensemble activation patterns for pairs of days, across the cells in each mouse we computed the Spearman correlation coefficient between the green/red emission ratios on the two days in consideration.

We performed statistical analyses using Prism (Graphpad) software. We used the Spearman correlation coefficient to assess the similarity in each mouse's ensemble patterns of green/red fluorescence ratios across pairs of time points. Box and whiskers plots show ranges of values determined across the mice in each experimental group, except that Figures 7D, 7E,and S1A show ranges across the specified sets of cells. Whiskers span the full range of a distribution, boxes enclose the middle 50%, and horizontal lines denote median values.

DATA AND SOFTWARE AVAILABILITY

Datasets will be made available upon reasonable request.